



Filtered-OFDM with channel coding based on T-distribution noise for underwater acoustic communication

Mustafa Sami Ahmed¹ · Nor Shahida Mohd Shah² · Fayad Ghawbar² · Yasir Amer Jawhar¹ · Akram A. Almohammed³

Received: 10 October 2019 / Accepted: 7 January 2020 / Published online: 14 January 2020
© Springer-Verlag GmbH Germany, part of Springer Nature 2020

Abstract

Bit error rate (BER) is typically high in underwater acoustic (UWA) channel, which is characterized by high propagation delay and poor quality of communications. UWA noise statistics do not follow the standard Gaussian distribution. It has been proven through field tests that the noise follows the t-distribution in Malaysian shallow-water. In this paper, a study on UWA error performance is presented based on t-distribution. Furthermore, the expressions of error performance are derived using binary phase shift keying (BPSK) and quadrature phase shift keying (QPSK) modulations order. Moreover, the new waveform filtered orthogonal frequency division multiplexing (F-OFDM) in UWA with turbo and convolution code is adopted. The simulation results show that at BER 10^{-3} , the Signal-to-Noise Ratio (SNR) is 6 dB and 11 dB for BPSK and QPSK, respectively. The turbo code performance appears to be superior over the convolution code. Furthermore, the results indicate that F-OFDM significantly improves the power spectral density to approximately 120 dBW compared with OFDM.

Keywords F-OFDM · OFDM · t-Distribution · Gaussian distribution · Channel coding · Underwater acoustic

1 Introduction

The efficiency of underwater communication is essential in various applications such as oil exploration, oceanographic studies and military applications. Therefore, underwater acoustic (UWA) communication system plays a vital role in such applications due to its significant performance compared to other communication systems (Sha'ameri et al. 2014). In wireless communications, UWA is a very challenging channel especially the shallow types. This is because they are highly influenced by various factors such as low data rate, limited bandwidth, severe multipath interference, strong fading and substantial Doppler shifts (Chen et al. 2017; Chitre et al. 2005; Gomathi and Manickam 2016; Javaid et al. 2019). Sound waves possesses lower attenuation compared with electromagnetic signals, hence, the reason for its preference in suitable applications. In addition, electromagnetic signals are characterized by high rate of absorption in ocean, sea or shallow waters. Therefore, electromagnetic signals are not an effective solution for underwater communications. On the other hand, optical communications have additional limitations in underwater due to particle suspension in seawater and the ambient light in the upper water column which severely scatter the optical signals resulting

✉ Mustafa Sami Ahmed
mustafa_sami87@yahoo.com

Nor Shahida Mohd Shah
shahida@uthm.edu.my

Fayad Ghawbar
fay_mh600@yahoo.com

Yasir Amer Jawhar
free_cccc@yahoo.com

Akram A. Almohammed
akrama2810@gmail.com

¹ Department of Communication Engineering, Faculty of Electrical and Electronic Engineering, Universiti Tun Hussein Onn Malaysia, Batu Pahat, 86400 Parit Raja, Johor, Malaysia

² Faculty of Engineering Technology, Universiti Tun Hussein Onn Malaysia, Pagoh Edu Hub, Panchor, Muar, 84600 Pagoh, Johor, Malaysia

³ Department of Computer and Communication Engineering, University Putra Malaysia, Seri Kembangan, Malaysia

in an inefficient communication (Babar et al. 2016; Qiao et al. 2017). Therefore, acoustic communication system is an enabling substantial technology for underwater wireless signal propagations. However, UWA channel poses high BER which could result in poor communication quality and high propagation delay (Liu et al. 2009).

In signal processing, Gaussian distribution possesses significant properties with low computational complexity and the white Gaussian noise is used for background noise. On the other hand, there are several noises in UWA channel such as radiation noise, environmental noise and targets self-noise etc. In practical applications, these complex noises, which are considered as non-Gaussian, increase the probability error of codewords at the communication system receiver (Li et al. 2017). Several researchers found that UWA channel does not follow the white Gaussian distribution (Al-Aboosi and Sha'ameri 2017b; Banerjee and Agrawal 2013, 2014; Chitre et al. 2004; Li et al. 2017; Panaro et al. 2012).

The noise characteristics, in terms of type and performance, is determined using probability density function (PDF) with a wide tail and an impulsive behaviour (Shah et al. 2018). T-distribution is a popular model that presents wider tails properties compared to Gaussian distribution (Al-Aboosi and Sha'ameri 2017b; Panaro et al. 2012; Shah et al. 2018). Another proposed non-Gaussian model is the Gaussian Mixture (GM) model which is widespread due to its "universal approximation" properties (Banerjee and Agrawal 2014). In Li et al. (2017), it was verified that the proposed algorithm based on Gaussian mixture model can estimate the PDF of noise. Another study has found that the noise distribution in shallow water follows the symmetric α -stable for snapping shrimp dominated ambient noise with a parameter characteristic of 1.69 and a scale parameter $6.8 \times 10^4 \mu\text{Pa}$ (Chitre et al. 2004). On the other hand, several researchers assumed that the noise distribution in UWA follows the Gaussian distribution which is not accurate (Al-Aboosi et al. 2017a, b; Goalic et al. 2006; Gomathi and Manickam 2016; Huang et al. 2008). As mentioned above, in underwater communication, the BER is high due to the non-white and non-Gaussian noise properties (Al-Aboosi and Sha'ameri 2017a).

Several studies have been conducted to reduce the BER in UWA communication using channel coding (Balfaqih et al. 2015; Huang et al. 2008; Jin et al. 2016; Liu et al. 2009). As for instance, convolution codes and Reed Solomon (RS) have been examined for UWA. However, additive white Gaussian noise is employed (Goalic et al. 2006). For spatial multiplexing in a single carrier underwater system, turbo codes have been tested with multiple transmitters (Roy et al. 2007). Furthermore, for single carrier transmission with a classical adaptive receiver, trellis coded modulations have been applied (Stojanovic et al. 1994). Another study in (Liu et al. 2017) proposed an UWA communication system

based on convolution code, repeat accumulate (RA) code, turbo code, and low-density parity-check (LDPC) code. The study (Liu et al. 2017a, b) indicates a significant reduction in BER presented by LDPC, RA and Turbo code. However, additive white Gaussian noise is utilized. Turbo code has higher flexibility and lower iteration rate compared with LDPC, which needs long package while UWA communication supports the use of short package. Nonetheless, both coding presents high algorithm complexity. On the other hand, Turbo code has higher reliability with better error correction rate compared with RA code (Liu et al. 2009). Turbo codes in telecommunication applications efficiently outperform the conventional codes as it provides better coding gain compared with un-coded channel and Viterbi/reed Solomon. Furthermore, the efficiency of turbo codes has an essential impact in telecommunication applications either by increasing the signal range or decreasing the transmission power of the signal. The turbo code equally presents high algorithm complexity of decoding with time delay and needs an interleaver (Han et al. 2009). Despite the efficiency of channel coding, it reduces the effective data rate (Chitre et al. 2005; Wu et al. 2018).

In communication systems, orthogonal frequency division multiplexing (OFDM) has been widely adopted due to its significant characteristic of dealing with high rate of transmissions over long channels (Almohammed et al. 2017; Babar et al. 2016; Chen et al. 2017; Chitre et al. 2005). OFDM splits the bandwidth into many subbands to get a longer symbol duration compared to channel multipath spread. Therefore, channel equalization complexity at the receiver is reduced as inter-symbol-interference (ISI) is neglected. In OFDM, the equalizer can be a single-tap filter for each subband by introducing a cyclic prefix (CP) that is greater than the longest multipath fading. However, OFDM has a high peak-to-average power ratio (PAPR) which causes transmission range reduction (Huang et al. 2008; Jawhar et al. 2019; Qiao et al. 2017). Numerous studies have investigated improving the performance of PAPR using different reduction techniques such as selective mapping methods, pre-coding, clipping method, proper insertion of interleaver and partial transmit sequence (PTS) (Huang et al. 2008; Jawhar et al. 2018).

Moreover, several studies have exposed the importance of F-OFDM (Wu et al. 2016; Liu et al. 2017a, b; Zhang et al. 2015). F-OFDM waveform is a promising 5G candidate (Balfaqih et al. 2017; Zhang et al. 2015) that can accomplish various features such as out of band (OOB) suppression, supporting asynchronous transmission, PAPR reduction, spectral efficiency improvement and design simplicity (Gerzaguet et al. 2017; Wang et al. 2017). A resource block (RB) filtered OFDM (RB-F-OFDM) has been designed to be scalable and modular at the same time (Noguet et al. 2011). Furthermore, the study in (Noguet et al. 2011) indicates that

RB-F-OFDM and F-OFDM have a similar performance which both offer a viable solution for dynamic spectrum sharing systems. Wu et al. (2016) observed that by applying F-OFDM, the guard bands are used to protect the samples from interference with each other, this technique is applied at the OFDM system and it wastes about 10% of the band. In the F-OFDM, the filtering operation saves the bandwidth spectrum due to the reduction in the guard band between the symbols by removing the sidelobes of the signal. Therefore, this operation leads to provide more bandwidth spectrum that can be used to carry out the useful data and then increase the data rate of the system (Zhang et al. 2015).

In this paper, F-OFDM is adopted in UWA to effectively improve the PSD compared to OFDM. Furthermore, various coding techniques with various constellation schemes of Phase-Shift Keying (PSK) are applied in the UWA system. In addition, this study presents the expression of error performance of Binary PSK (BPSK) and Quadrature PSK (QPSK) constellation based on t-distribution. The rest of the paper is organized as follows: Sect. 2 introduces the channel model of UWA which consists of the data collection and the noise processing flow. Section 3 presents the derivation of error probability expression for BPSK and QPSK. Section 4 describes the channel coding techniques to reduce the BER. Section 5 Presents the F-OFDM waveform in UWA including the system and filter design. The outcomes were discussed in Sect. 6. The conclusion for the work is stated in Sect. 7.

2 Channel modeling of UWA

In this model, the channel characteristics is analyzed using the fitting tool in MATLAB. Based on this analysis, the expressions for error probability of BPSK and QPSK is derived.

2.1 Data collection in underwater acoustic

Underwater acoustic noise (UWAN) samples were obtained directly from the underwater environment. The samples were collected at depths of 4 m and 12 m from the seafloor from shallow water at Senggarang, Batu Pahat, Johor, Malaysia ($1^{\circ} 49' 21.8''$ N $102^{\circ} 50' 14.3''$ E) on 16 May 2018. The segment was received through a broadband hydrophone (7 Hz ~ 22 kHz) model Dolphin Ear 200 Series. Figure 1 depicts the experiment site located about 2.4 km from the shore. During the daytime, the wind speed was about 7 Knots and the temperature at the surface of the sea was approximately 29°C measured using TDS-3. One sample of length 20 s was collected at each depth, while the salinity was 35 ppt and the pH was 7.8. Similarly, the speed of sound depends on the salinity, wind speed, the depth and to the temperature as shown in Medwin equation (Eq. 1). Therefore, these factors have direct impact on the speed of sound propagation as it shows temporal and spatial variability in UWA communication (Al-Aboosi et al. 2017a, b; Medwin and Clay 1997; Murugan and Natarajan 2010).

$$c = 1449.2 + 4.6T - 0.055T^2 + 0.00029T^3 + (1.34 - 0.01T)(S - 35) + 0.016h \quad (1)$$

where the speed of sound c the temperature T is expressed in $^{\circ}\text{C}$, salinity S in parts per thousand (ppt) and depth h in meters. Equation 1 is valid for: $0^{\circ} \leq T \leq 35^{\circ}\text{C}$, $0 \leq S \leq 35$ ppt, and $0 \leq h \leq 1000$ m the speed of sound was 1543.48 m/s and 1543.61 m/s at depths 4 m and 12 m, respectively.

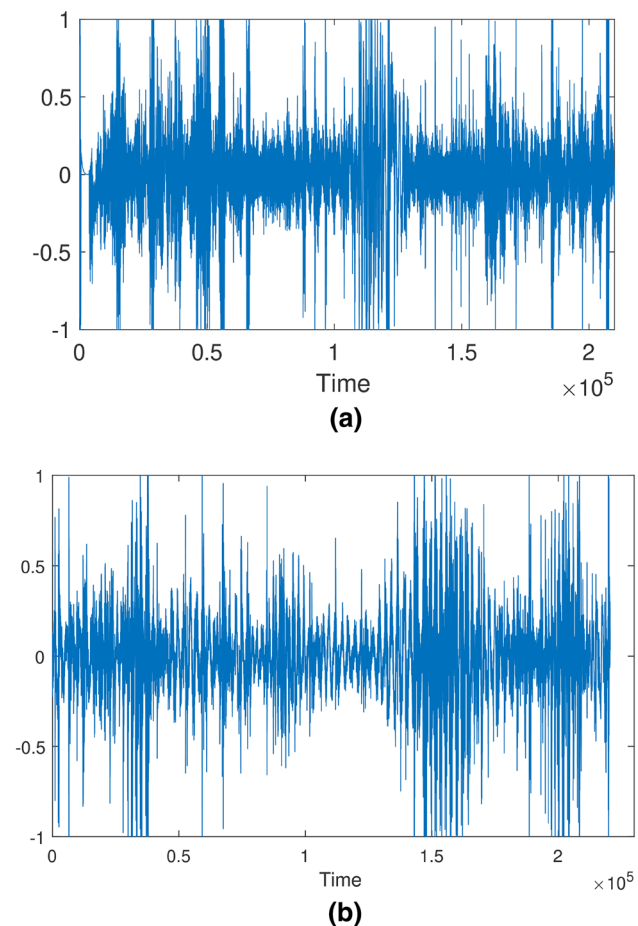
The hydrophone was used to record the UWAN and convert the samples into discrete time for more processing to be stored in a personal computer. The measurements are based on various depths. Table 1 displays the parameters specification for data collection. Figure 2 displays the time

Fig. 1 Experiment testing site



Table 1 Parameter specification for data collection

Parameter	Value
Location	(1° 49' 21.8" N 102° 50' 14.3" E)
Frequency range	7–22 kHz
Temperature surface	29 °C
Speed of wind	7 Knots
Salinity	35 ppt
Depth	4, 12 m
Sample of length	20 s

**Fig. 2** Time representation of the UWAN at depths of **a** 4 m and **b** 12 m

representation waveform of the collected UWAN data with two different depths of 4 m and 12 m.

2.2 Noise process flow

The distribution of the collected data is analyzed by applying Gaussian and t-distribution using the fitting tool in

MATLAB. By comparing the two distribution methods, it can be clearly seen that the amplitude of the UWAN follows the t-distribution, as shown in Fig. 3. Therefore, the assumption of Gaussian distribution is not applicable in UWAN.

Equation (2) demonstrates the t-distribution PDF (Ahsanullah et al. 2014);

$$\rho_{(l,d)} = \frac{\Gamma[(d+1)/2]}{\sqrt{\pi d} \Gamma(d/2)} \left(1 + \frac{l^2}{d}\right)^{-\frac{(d+1)}{2}}, \quad (2)$$

where $\Gamma(\cdot)$ is the gamma function and d is the degree of freedom that regulates the distribution dispersion. $\rho(l, d)$ is the probability of observing a particular value of l from a t-distribution with d . The PDF represented in Eq. (2) has a zero mean and a variance equals to $d/(d-2)$, where $d \geq 2$. When the value of d is low, the tails of the PDF become wider and when the value is high, the tails become smaller and converge to the Gaussian distribution. The obtained values of d at the depths of 4 m and 12 m were 2.91 and 3.52 respectively for a short time of a few seconds. Based on this result, the UWAN is assumed to be stationary, thus the channel with space-variant multipath effects and time-variant Doppler shifts are ignored (Stojanovic and Preisig 2009; Urick 1984). Besides, the average is assumed as $d \cong 3$. The analysis indicates that UWAN characteristics do not follow the Additive white Gaussian noise (AWGN) and it shows that the PDF of the UWAN follows the t-distribution. However, for modelling a random variable X with variance $\sigma > 2$, the following changes of variables can be made.

$$l = \sqrt{\frac{d}{\sigma^2(d-2)}}x, \quad (3)$$

where X random variable X , σ is variance and accordingly, a new scaled PDF function can be written as:

$$f_T(x, d) = \frac{\Gamma\left[\frac{(d+1)}{2}\right]}{\sigma \sqrt{\pi(d-2)} \Gamma\left(\frac{d}{2}\right)} \left(1 + \frac{x^2}{\sigma^2(d-2)}\right)^{-\frac{(d+1)}{2}}, \quad (4)$$

where $f_T(x, d)$ is PDF function in UWA, For $d=3$, the PDF is:

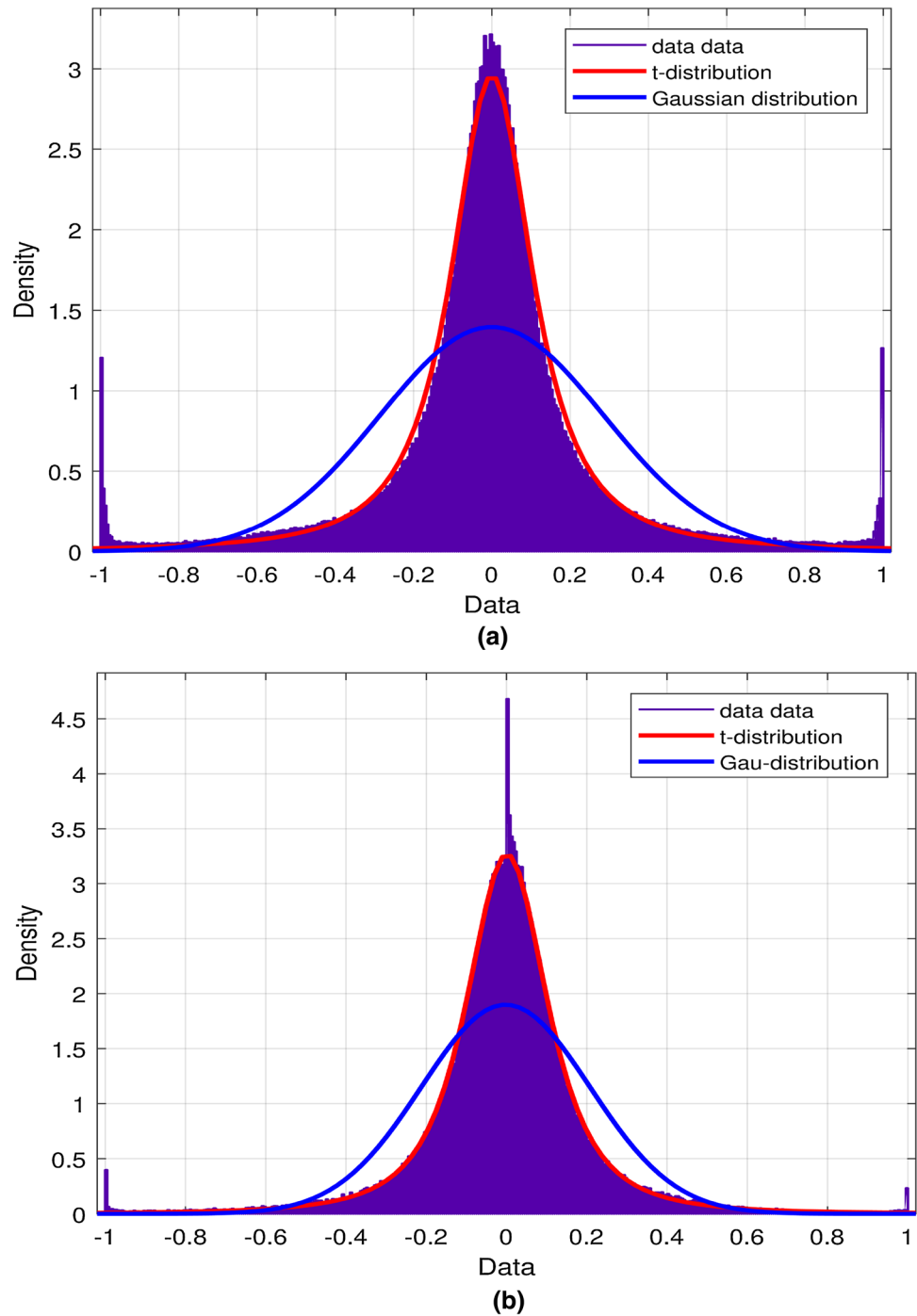
$$f_T(x, 3) = \frac{0.636}{\sigma} \left(1 + \frac{x^2}{\sigma^2}\right)^{-2} \quad (5)$$

and for $d=4$, the PDF can be:

$$f_T(x, 4) = \frac{0.534}{\sigma} \left(1 + \frac{x^2}{\sigma^2}\right)^{-2.5}, \quad (6)$$

where X is the random variable X , σ , the variance with $f_T(x, d)$ being the PDF in UWA, for $d=3$.

Fig. 3 The amplitude distribution of the UWAN with the Gaussian and t-distribution **a** 4 m and **b** 12 m



3 Error probability of UWA

Let us consider a communication system of UWA which transmits symbol $T(j)$, where j th is a point of a specific modulation order. At the receiver $R(j)$ and with the existence of noise only, the received signal is the summation of the transmitted signal and noise as given in Eq. (7).

$$R(j) = T(j) + N(j), \tag{7}$$

where N is the noise sample that belongs to t-distribution as presented in Eq. (5) and (6). The following subsections present the error probability of the different modulation orders of PSK.

3.1 BPSK constellation

According to the previous estimation of PDF, it is expected to evaluate an expression of the symbol error probability

for binary signal in the UWAN channel. The system model is presented as depicted in Fig. 4.

The derivation of the error performance is initiated using the BPSK signal with the transmitted symbols of BPSK given by $A_1 = \sqrt{E_b}$ and, $A_2 = -\sqrt{E_b}$ where E_b is the energy of bit. The d with a value of 3 can be defined as given in Eqs. (8) and (9).

$$p(T|A_1) = f(x + A_1) = \frac{0.636}{\sigma} \left(1 + \frac{(x + A_1)^2}{\sigma^2} \right)^{-2} \quad (8)$$

and,

$$p(T|A_2) = f(x - A_2) = \frac{0.636}{\sigma} \left(1 + \frac{(x - A_2)^2}{\sigma^2} \right)^{-2}. \quad (9)$$

Therefore, the symbol error probability for a binary equal probability source in the detection of an antipodal signal spoilt by additive noise can be calculated by integrating any of the possible functions as expressed in Eq. (10). Equation (11) satisfies $p(T_1) = p(T_0) = 0.5$.

$$P_{BPSK} = \frac{1}{2}p(T_1)p(e/T_1) + \frac{1}{2}p(T_0)p(e/T_0) \quad (10)$$

if $p(T_1) = p(T_0) = 0.5$, then:

$$P_{BPSK} = \int_0^\infty p(e/T_1)dx. \quad (11)$$

The energy per bit is introduced by $E_b = A^2T_b$ where T_b is the bit time duration. Furthermore, the noise average power spectral density is presented by $N_o = \sigma^2/B$, where $B = 1/2T_b$ is the occupied bandwidth at the baseband. Let us assume the amplitude of the pulses is unitary, i.e., $A = 1$ in the presence of zero generality loss. In addition, the noise variance σ^2 is related to the SNR (E_b/N_o), as shown in in Eq. (12).

$$\sigma^2 = \frac{1}{(2E_b/N_o)}. \quad (12)$$

Finally, by substituting Eq. (8) in Eq. (11), the probability of symbol error for the binary UWA channel for the d with a value of 3 can be written as Eq. (13). Similarly, for the d with a value of 4, the probability of symbol error for the binary UWA channel can be written as Eq. (14).

$$P_{BPSK} = 0.636 \sqrt{\frac{2E_b}{N_o}} \int_0^\infty \left[1 + \frac{2E_b}{N_o}(x + 1)^2 \right]^{-2} dx, \quad (13)$$

$$P_{BPSK} = 0.534 \sqrt{\frac{2E_b}{N_o}} \int_0^\infty \left[1 + \frac{2E_b}{N_o} \frac{(x + 1)^2}{2} \right]^{-2.5} dx. \quad (14)$$

3.2 QPSK constellation

The QPSK constellation is considered as two BPSK signals in phase quadrature. As noise does not statistically depend on quadrature components, the 2-bit symbol correct decision probability is given by Eq. (15) (Banerjee and Agrawal 2014).

$$P_c = (1 - P_2)^2, \quad (15)$$

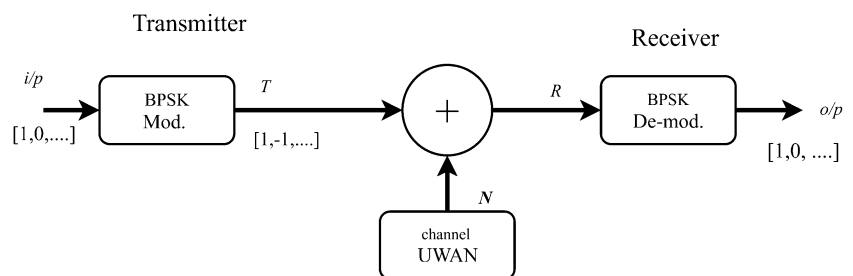
where P_2 is the symbol error probability for BPSK modulation order. Since $P_2 = P_{BPSK}$, the symbol error probability for QPSK is as contained in Eq. (16),

$$P_{QPSK} = 1 - P_c = 2P_{BPSK} \{1 - 0.5P_{BPSK}\}. \quad (16)$$

For $d=3$, we substitute Eq. (13) in (16), then the QPSK symbol error probability can be written as Eq. (17). Similarly, for $d=4$ Eq. (14) is substituted in (16) to give Eq. (18), the symbol error probability of the binary UWA channel.

$$P_{QPSK} = 1.272 \sqrt{\frac{2E_b}{N_o}} \int_0^\infty \left[1 + \frac{2E_b}{N_o}(x + 1)^2 \right]^{-2} dx \times \left[1 - 0.318 \sqrt{\frac{2E_b}{N_o}} \int_0^\infty \left[1 + \frac{2E_b}{N_o}(x + 1)^2 \right]^{-2} dx \right] \quad (17)$$

Fig. 4 BPSK transmitter–receiver block diagram (Shah et al. 2018)



$$P_{QPSK} = 1.068 \sqrt{\frac{2E_b}{N_o}} \int_0^\infty \left[1 + \frac{2E_b}{N_o} \frac{(x+1)^2}{2} \right]^{-2.5} dx$$

$$\times \left[1 - 0.267 \sqrt{\frac{2E_b}{N_o}} \int_0^\infty \left[1 + \frac{2E_b}{N_o} \frac{(x+1)^2}{2} \right]^{-2.5} dx \right]$$

(18)

4 Channel coding

To approach an efficient acoustic system with a highly improved communication link, channel coding is applied for correcting the system’s remaining errors. The main aim is to increase the BER reduction rate to an optimum level. In this study, two channel coding techniques, convolution and turbo codes have been investigated.

4.1 Convolution code

Convolutional codes (CC) are defined by three parameters (n, k, u) representing the number of output bits, input bits

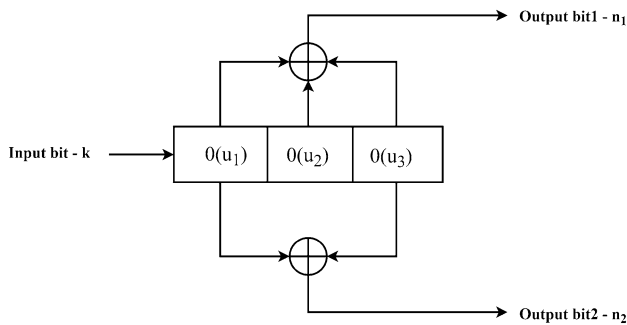


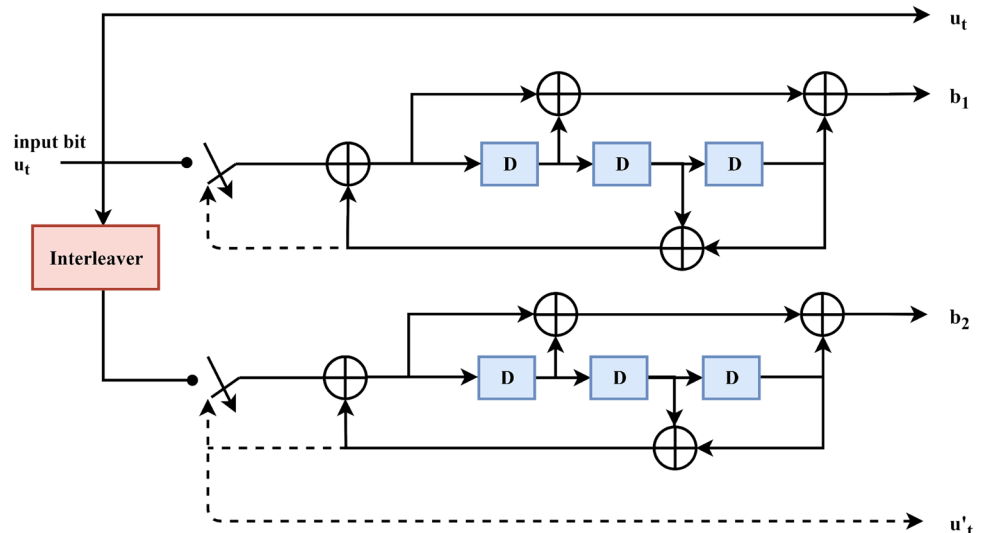
Fig. 5 Convolutional encoder structure

and the number of memory registers, respectively (Tahir et al. 2017). The code efficiency can be measured by the code rate $R=k/n$ where k and n are the range from 1 to 8 and 2 to 10, respectively. One CC was used which is defined as CC (7, 5). Viterbi algorithm is used for decoding using trellis representation with four states following the CC order. Hard or soft decoding is performed in which hard option uses only binary values, whereas the soft decoding uses real values generated by the output equalizer. There are several options for polynomials u -order code. Through the simulation and by using trial and error, the best polynomial can be obtained. In this work, two generator polynomials are applied, defined by the bits (1 1 1) and (1 0 1), as shown in Fig. 5 (Bernard 2001).

4.2 Turbo code

Turbo codes are generally made of two convolution encoders in parallel and are separated by an interleaver (Berrou et al. 1993). The goal is to construct the polynomial codes for individual encoders and to select a suitable interleaver. In the encoding process, the new element to be discussed and analysed is the interleaver since the individual encoders are basically considered as convolutional. A turbo encoder using an interleaver is presented in Fig. 6. The first encoder consists of a systematic stream output u_t and a parity stream b_1 , while the second individual encoder only consists of a parity stream b_2 resulting in 1/3 turbo code. Furthermore, it is important to know the first states and the last states of the encoder to avoid any performance loss, and that is performed by trellis termination. Therefore, trellis termination of turbo code is necessary to achieve a good performance especially in UWA with short information blocks represented by the dashed zone of Fig. 6. At the decoding part, the turbo decoder is represented by two soft-input-soft-output

Fig. 6 Turbo code structure (Tahir et al. 2017)



(SISO) decoders. The structure of turbo decoders is almost like the convolutional decoder with some changes. The first decoder consists of a systematic stream and the first parity stream, while the second decoder consists of an interleaver of the systematic stream and the second parity stream. The decoding iterative scheme consists of essential A posteriori probability (APP) decoder, an interleaver and deinterleaver (Tahir et al. 2017).

5 Applying filtered-OFDM

F-OFDM is recommended as one of the waveform framework candidates for 5G communication. It is designed with a filter over the entire frequency bandwidth to accomplish the desirable frequency localization for 5G applications. The out-of-band (OOB) suppressing, asynchronous transmission and low latency are the distinctive features of the filtered-based waveform frameworks. In this section, the F-OFDM candidate is applied to the UWA system to improve the BER performance and spectral efficiency.

5.1 System design

Figure 7 illustrates the underwater acoustic system (UWAS) based on F-OFDM, where the input data sequence X is encoded initially to generate the encoded data sequence X' . Thereafter, various PSK modulation family is used to map X' . Next, the baseband data is oversampled by inserting zeroes between the samples. After that, the Inverse Fast Fourier Transform (IFFT) is utilized to convert the data sequence from frequency domain to time domain using Eq. (19).

$$x(n) = \frac{1}{\sqrt{N}} \sum_{k=0}^{N-1} X'_k e^{j2\pi kn/N} \quad 0 \leq n \leq N-1. \quad (19)$$

The OFDM signal in the time domain is then expanded by CP operation where the CP has a 7–25% from the total data (Hammoodi et al. 2019; Ochiai and Imai 2001). Lastly, the OFDM signal $x(n)$ is passed to the transmitter filter $f(n)$ to produce the F-OFDM transmitting signal $g(n)$ (Eq. 20).

$$g(n) = x(n) \times f(n). \quad (20)$$

At the receiver side, the received signal is passed to the matched filter (Wu et al. 2016). Subsequently, the serial data are converted into parallel and the cyclic prefix is removed. Next, the data sequence is converted from the time domain into the frequency domain using Fast Fourier Transform (FFT). After that, the oversampling is removed, the parallel signal is then converted into serial data, and then various PSK demodulation is applied. Finally, the decoding is performed to recover the encoded input data stream.

5.2 Filter design

In F-OFDM, filter design plays an important role in achieving frequency localization on the signal as well as achieving more flexibility between the time and frequency localization, since the desired frequency-domain localization leads to dispersion in the time-domain (Gerzaguet et al. 2017). In OFDM system, the signal is a rectangular pulse shape (*sinc* function); therefore, this leads to large sidelobes for both sides of the signal in frequency-domain. Consequently, the frequency spectrum is not accurately localized. In F-OFDM, *sinc* impulse response filter, i.e., low pass filter (LPF) is a

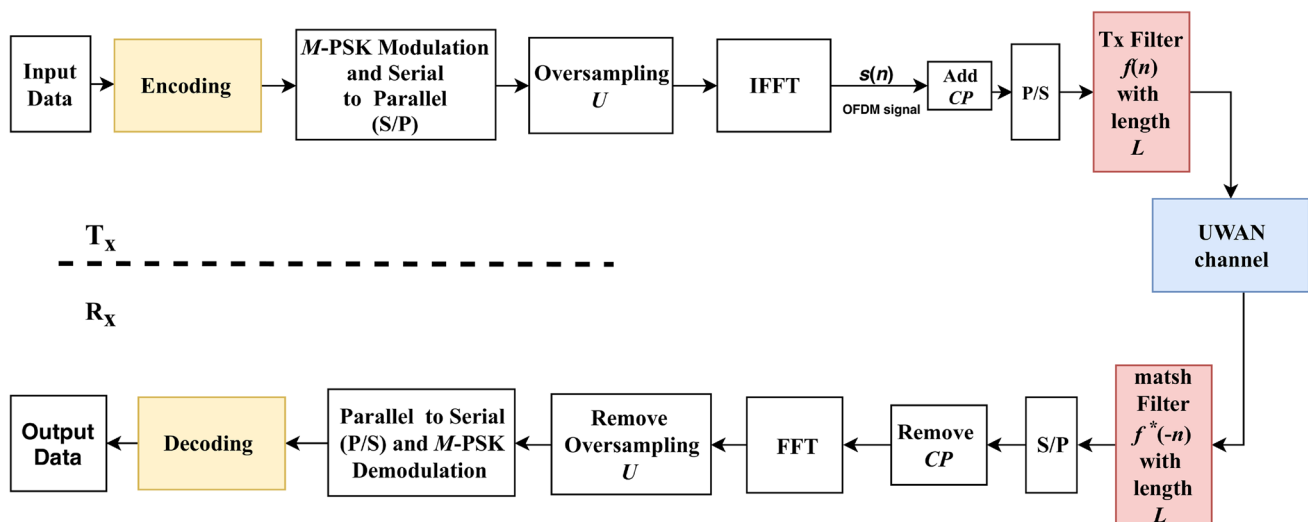


Fig. 7 Block diagram of UWAS based F-OFDM

suitable spectrum shaping filter for the F-OFDM system due to its ability to suppress OOB, and it causes no distortion in the passband of the signal. Moreover, time windowing mask is applied to provide a good time localization and to ensure smooth transitions for both ends of the filter impulse response (Wang et al. 2017). The finite impulse response (FIR) filter is designed by multiplying the infinite impulse response of the low pass filter (LPF) with a finite time-domain window (Wu et al. 2016). Therefore, the *sinc* impulse response filter in the time-domain is as expressed in Eq. (21).

$$f(n) = h_{LPF}(n) \cdot w(n) \tag{21}$$

with

$$h_{LPF}(n) = \frac{\sin(w_c \cdot n)}{w_c \cdot n}, \tag{22}$$

where $h_{LPF}(n)$ represents the *sinc* impulse response of the LPF, and w_c is the cut-off frequency of the LPF, $w(n)$ denotes the impulse response of the windowing mask. In addition, adopting a suitable window function can provide a flexible trade-off between frequency and time localization. Hence, the ISI can be limited to an acceptable level. The rooted raised cosine (RRC) window function appears to be suitable for F-OFDM since it is more flexible than other window functions such as presented by Remez and Hanning (Wu et al. 2016). Therefore, the time response of the RRC window is formulated as given in Eq. (23) (Wu et al. 2016).

$$w_{RRC}(n) = \left[0.5 \left(1 + \cos \left(\frac{2\pi n}{L-1} \right) \right) \right]^\alpha, \tag{23}$$

where L symbolizes the filter length which is equals to half of OFDM symbol length plus 1, and α stands for the roll-off factor which is the parameter that controls the window shape, and it's limited to $0 \leq \alpha \leq 1$. When $\alpha = 1$, the window is hamming, and when $\alpha = 0$, the window is rectangular as

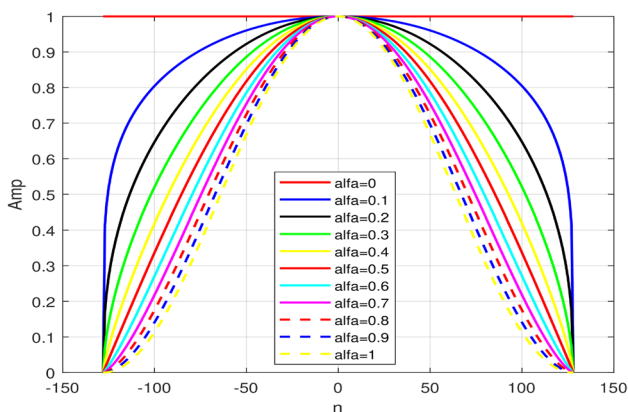


Fig. 8 Window of pass band with various roll-off factors

depicted in Fig. 8. The filter length of F-OFDM is let to exceed the *CP* length to achieve more flexibility for the filter design and to accomplish a significant balance between the frequency and the time localization (Schaich and Wild 2014). However, the roll-off factor of the RRC window provides additional freedom to achieve the frequency and the time localization balance as well. As a result, the RRC window is more suitable for the F-OFDM system compared to other windows.

6 Results and discussion

In this section, the evaluation of UWA communication system is introduced based on two main factors. Firstly, the error performance is evaluated and compared with SNR. Secondly, the F-OFDM and OFDM are analyzed and compared with reference to the PSD. The results are obtained using MATLAB simulation in the presence of additive t-distribution noise with d value of 3 and 4 as obtained from the fitting tool. The rate of the convolution and turbo code is set to 1/2 and 1/3, respectively within hard decoding which shows highly efficient performance compared with other rates as explained in the literature.

6.1 BER performance

The simulation and theory in a single carrier are presented and then BER is compared with E_b/N_o as shown in Figs. 9 and 10 which illustrate the BPSK and QPSK, respectively. The simulation data are represented by the blue line and the theoretical BER for the un-coded system is represented by the red line for t-distribution. On the other hand, the black line represents Gaussian distribution. The Points plotted on the *y-axis* have a BER $\leq 10^{-4}$. The result obviously shows

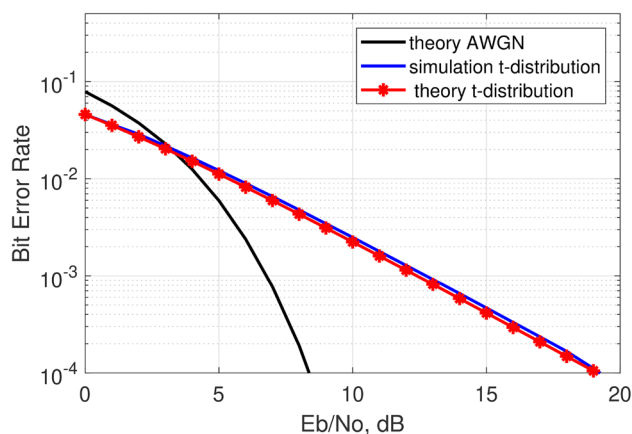


Fig. 9 Error performance for BPSK under UWA and AWGN channels with $d=3$

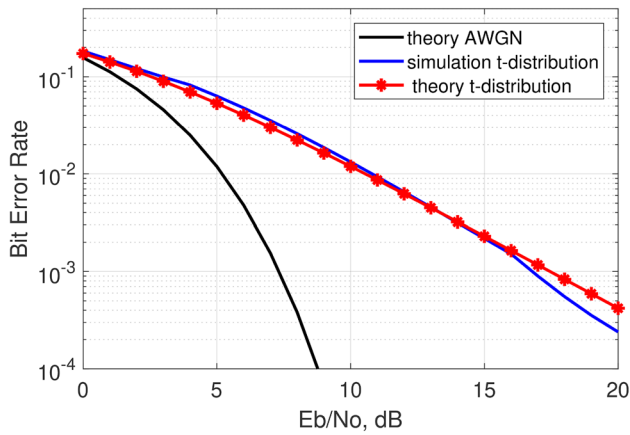


Fig. 10 Error performance for QPSK under UWAN and AWGN channels with $d=3$

that the theoretical BER and simulation data are identical to each other. This means the t-distribution channel that has been performed in the simulation is identical with the theoretical calculation. Furthermore, the BER performance of the signal based on the t-distribution is less than that based on the Gaussian distribution (AWGN). Moreover, at BER 10^{-3} , the SNR is as 6 dB and 11 dB for BPSK and QPSK, respectively. Furthermore, it can be noticed that the BER in BPSK has better performance than QPSK with 3 dB at BER of 10^{-3} because the points of constellation has become closer to each other.

By comparing Fig. 11 with Fig. 9, the BER is improved by approximately 1 dB at BER of 0.02 when d is increased because the t-distribution converges to the Gaussian distribution. In this part, F-OFDM and OFDM performance are evaluated in terms of BER. Figure 12a illustrates the simulation results of BER for both F-OFDM and OFDM waveform employing the turbo and convolution codes. In

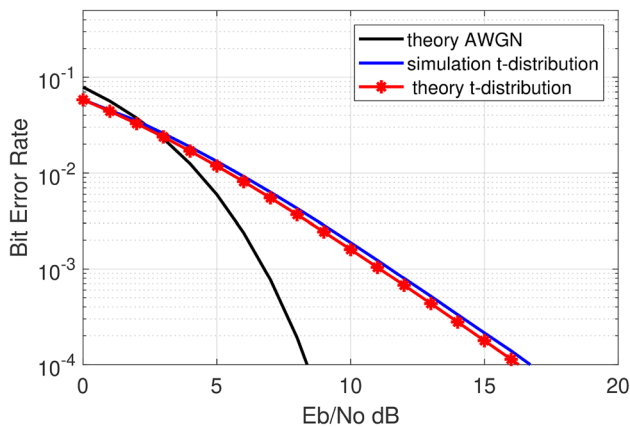


Fig. 11 Error performance for BPSK under UWAN and AWGN channels with $d=4$

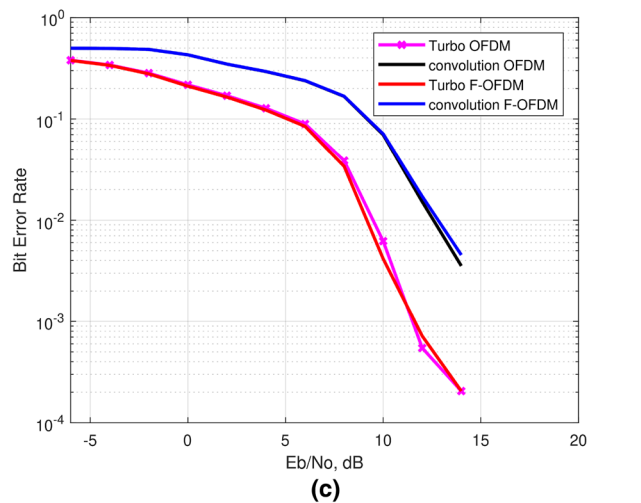
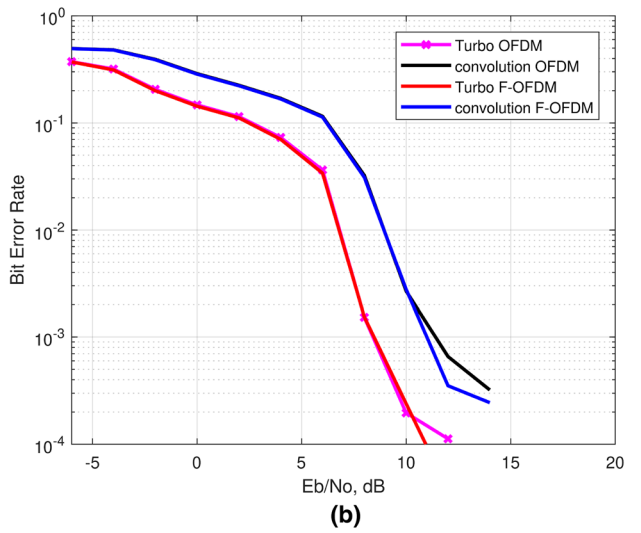
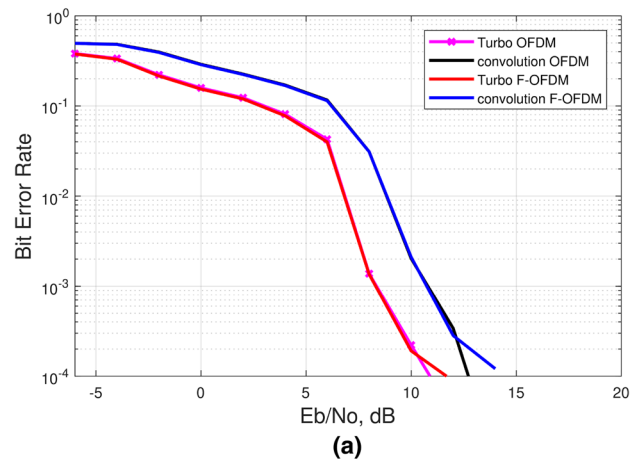


Fig. 12 Comparison BER of F-OFDM and OFDM for $d=3$ **a** BPSK **b** QPSK and **c** 16-PSK

addition, BPSK is considered as the modulation order for the systems applied in this simulation and 256 is set as the number of subcarriers. Based on the simulation in Fig. 11, it is clearly demonstrated that BER of F-OFDM and OFDM is identical at all values of SNR. According to the obtained results from Fig. 12b, c compared with Fig. 12a, it is obvious that the BER performance depends on the modulation order, where high modulation order degrades the BER performance due to its sensitivity to interference.

On the other hand, the BER performance of the turbo and the convolution code were compared based on t-distribution and the degree of freedom equal 3. The simulation results show that the turbo code performance is more significant than the convolution code, as depicted in Fig. 12a–c. The improvement of BER of turbo code compared to convolution code at BPSK, QPSK and 16 PSK is approximately 2 dB at BER 10^{-3} . Therefore, turbo code is suitable for UWA channel. However, related studies indicate that turbo code has complexity in terms of implementation.

Conversely, Fig. 13a–c represent the BER performance of the UWA system based on OFDM and F-OFDM systems when $d=4$. Clearly, the BER performance of the system is improved when increasing the value of d as the PDF of t-distribution becomes closer to the Gaussian distribution. In other words, when the value of d is low, the tails of the PDF become wider and when the value is high, the tails becomes narrow and converge to the Gaussian distribution.

In UWA channel, previous work deployed AWGN while noise channel does not follow the Gaussian distribution. However, in this work, the experimental results show that the noise channel follows the t-distribution, which affects the performance of channel coding techniques.

6.2 PSD performance

The main advantage of filtered waveforms is its significantly reduced OOB which helps support asynchronous transmissions. Therefore, it is essential to validate the performance by comparing the OOB of standard OFDM with different waveforms. The PSD is used to evaluate the frequency localization of OFDM and F-OFDM by comparing each waveform's PSD. In F-OFDM, the filter is designed with filter length, $L=257$, and the roll-off factor $\alpha=0.6$. Figures 14 and 15 indicate the PSD of the OFDM and F-OFDM waveforms for convolution and turbo codes, respectively, where the OOB power of the OFDM stander is -44 dBW and -46 dBW for convolution and turbo code correspondingly, whereas the OOB power of the F-OFDM waveform is -165 dBW and -166 dBW for convolution and turbo code. The results demonstrate that the F-OFDM outperforms the OFDM with OOB power reduction at approximately 120 dBW. Furthermore, it shows that both convolution and

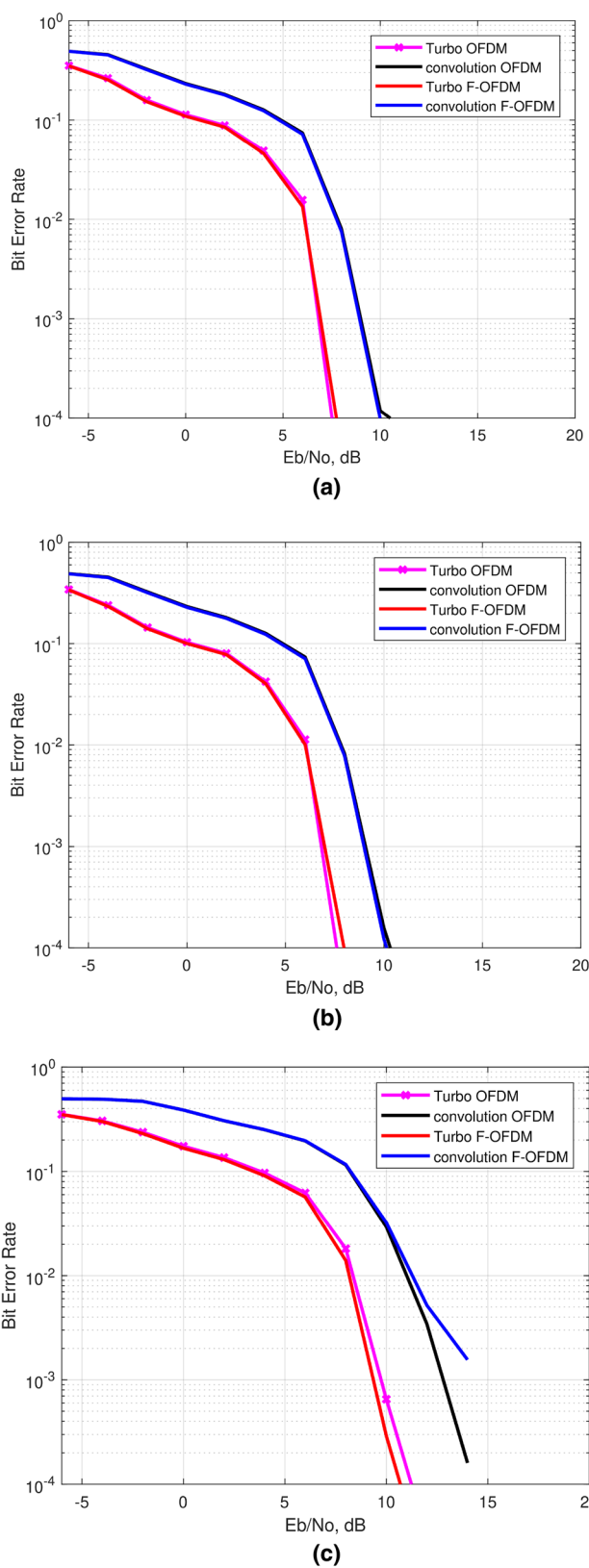


Fig. 13 Comparison BER of F-OFDM and OFDM for $d=4$ a BPSK b QPSK and c 16-PSK

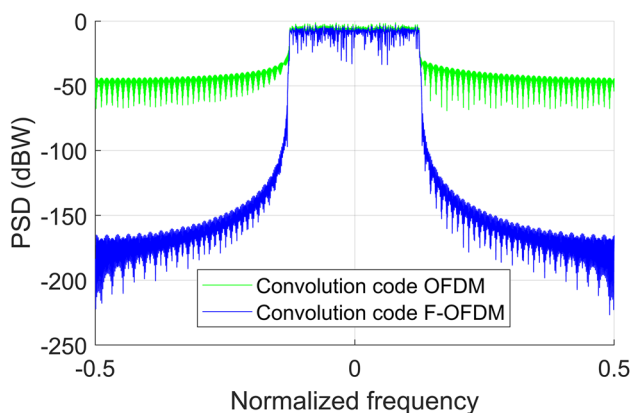


Fig. 14 PSD of OFDM and F-OFDM waveforms under convolution code

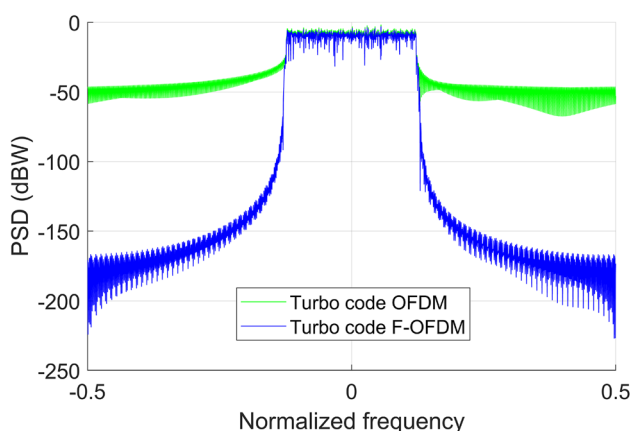


Fig. 15 PSD of OFDM and F-OFDM waveforms under turbo code

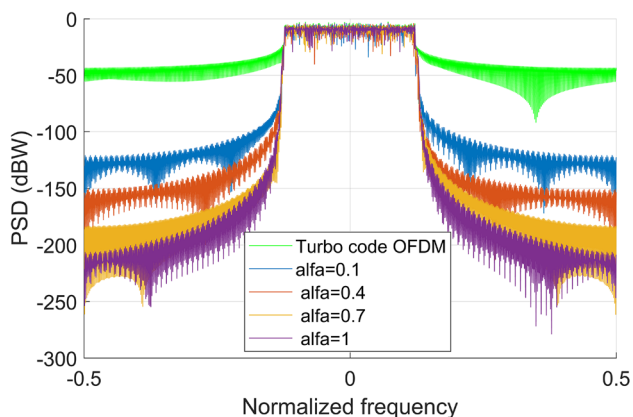


Fig. 16 Comparison PSD of F-OFDM and OFDM with different α

turbo code do not have a large impact on OOB. Therefore, the F-OFDM waveform has a better level of frequency localization.

Figure 16 presents an example of the impact of α on OOB; it is apparent that increasing the α value, improves the OOB overwhelming performance. On the other hand, when α value is increased, the OOB performance is significantly improved and vice versa. However, when α reaches a maximum value, it affects the passband edge and sharper. Therefore, α value is selected to be 0.6 in this simulation.

7 Conclusion

In conclusion, there are several applications requiring solutions to the interferences posed by UWA channels. This includes the high BER which degrades the system performance. Experimental field tests and analysis on a shallow water medium has shown that UWA channel noise follows t-distribution. Firstly, the turbo and convolution codes for UWA were compared and verified. The simulation results indicate that the turbo code outperforms the convolution code and it is more suitable in UWA with the cost of high computational complexity. Furthermore, the results also show the possibility of increasing the data rate by employing F-OFDM instead of OFDM due to the reduction of OOB. Consequently, there is no need to impose any guard between neighbouring subcarriers. However, F-OFDM increases the system's computational complexity due to the added filter. For future work, polar code is recommended to be applied for BER reduction performance due to its low complexity.

Acknowledgements This research was funded by the Ministry of Higher Education Malaysia under Fundamental Research Grant Scheme Vot No. K096 and partially sponsored by Universiti Tun Hussein Onn Malaysia

References

- Ahsanullah M, Kibria BG, Shakil M (2014) Normal and student's t distributions and their applications, vol 4. Springer, New York
- Al-Aboosi YY, Sha'ameri AZ (2017a) Improved signal de-noising in underwater acoustic noise using S-transform: a performance evaluation and comparison with the wavelet transform. *J Ocean Eng Sci* 2(3):172–185
- Al-Aboosi YY, Sha'ameri AZ (2017b) Improved underwater signal detection using efficient time–frequency de-noising technique and pre-whitening filter. *Appl Acoust* 123:93–106
- Al-Aboosi YY, Ahmed MS, Shah NSM, Khamis NHH (2017a) Study of absorption loss effects on acoustic wave propagation in shallow water using different empirical models. *ARPN J Eng Appl Sci* 12:6474–6478
- Al-Aboosi YY, Kanaa A, Sha'ameri AZ, Abdualnabi HA (2017b) Diurnal variability of underwater acoustic noise characteristics in shallow water. *Telkomnika* 15(1):314
- Almohammed AA, Noordin NK, Sali A, Hashim F, Balfaqih M (2017) An adaptive multi-channel assignment and coordination scheme

- for IEEE 802.11 P/1609.4 in vehicular Ad-Hoc networks. *IEEE Access* 6:2781–2802
- Babar Z, Sun Z, Ma L, Qiao G (2016) Shallow water acoustic channel modeling and OFDM simulations. In: Paper presented at the OCEANS 2016 MTS/IEEE Monterey
- Balfaqih M, Nordin R, Balfaqih Z, Haseeb S, Hashim A (2015) An evaluation of IEEE 802.11 MAC layer handoff process in capwap centralized WLAN. *J Theor Appl Inf Technol* 71(3):468–479
- Balfaqih M, Ismail M, Nordin R, Balfaqih Z (2017) Handover performance evaluation of centralized and distributed network-based mobility management in vehicular urban environment. In: Paper presented at the 2017 9th IEEE-GCC conference and exhibition (GCCCE)
- Banerjee S, Agrawal M (2013) Underwater acoustic noise with generalized Gaussian statistics: effects on error performance. In: Paper presented at the OCEANS-Bergen, 2013 MTS/IEEE
- Banerjee S, Agrawal M (2014) On the performance of underwater communication system in noise with Gaussian mixture statistics. In: Paper presented at the communications (NCC), 2014 twentieth national conference on
- Bernard S (2001) *Digital communications fundamentals and applications*. Prentice Hall, Upper Saddle River
- Berrou C, Glavieux A, Thitimajshima P (1993) Near Shannon limit error-correcting coding and decoding: Turbo-codes. In: Paper presented at the communications, 1993. ICC'93 Geneva. Technical program, conference record, IEEE international conference on
- Chen P, Rong Y, Nordholm S, He Z, Duncan AJ (2017) Joint channel estimation and impulsive noise mitigation in underwater acoustic OFDM communication systems. *IEEE Trans Wirel Commun* 16(9):6165–6178
- Chitre M, Potter J, Heng OS (2004) Underwater acoustic channel characterisation for medium-range shallow water communications. In: Paper presented at the OCEANS'04. MTTs/IEEE TECHNO-OCEAN'04
- Chitre M, Ong S, Potter J (2005) Performance of coded OFDM in very shallow water channels and snapping shrimp noise. In: Paper presented at the OCEANS, 2005. Proceedings of MTS/IEEE
- Wu D, Zhang X, Qiu J, Gu L, Saito Y, Benjebbour A, Kishiyama Y (2016) A field trial of f-OFDM toward 5G. In: *IEEE globecom workshops (GC Wkshps)*, pp 1–6
- Gerzaguat R, Bartzoudis N, Baltar LG, Berg V, Doré J-B, Ktésas D et al (2017) The 5G candidate waveform race: a comparison of complexity and performance. *EURASIP J Wirel Commun Netw* 2017(1):13
- Goalic A, Trubuil J, Beuzelin N (2006) Channel coding for underwater acoustic communication system. In: Paper presented at the OCEANS 2006
- Gomathi R, Manickam JML (2016) PAPR reduction technique using combined DCT and LDPC based OFDM system for underwater acoustic communication. *ARPJ J Eng Appl Sci* 11(7):4424–4430
- Hammoodi A, Audah L, Taher MA (2019) Green coexistence for 5G waveform candidates: a review. *IEEE Access* 7:10103–10126
- Han W, Huang J, Jiang M (2009) Performance analysis of underwater digital speech communication system based on LDPC codes. In: Paper presented at the industrial electronics and applications, 2009. ICIEA 2009. 4th IEEE Conference on
- Huang J, Zhou S, Willett P (2008) Nonbinary LDPC coding for multicarrier underwater acoustic communication. *IEEE J Sel Areas Commun* 26(9):1684–1696
- Javaid N, Ahmad Z, Sher A, Wadud Z, Khan ZA, Ahmed SH (2019) Fair energy management with void hole avoidance in intelligent heterogeneous underwater WSNs. *J Ambient Intell Humaniz Comput* 10(11):4225–4241
- Jawhar YA, Ramli KN, Taher MA, Shah NSM, Audah L, Ahmed MS, Abbas T (2018) New low-complexity segmentation scheme for the partial transmit sequence technique for reducing the high PAPR value in OFDM systems. *ETRI J* 40(6):699–713
- Jawhar YA, Audah L, Taher MA, Ramli KN, Shah NSM, Musa M, Ahmed MS (2019) A review of partial transmit sequence for PAPR reduction in the OFDM systems. *IEEE Access* 7:18021–18041
- Jin L, Li Y, Zhao C, Wei Z, Li B, Shi J (2016) Cascading polar coding and LT coding for radar and sonar networks. *EURASIP J Wirel Commun Netw* 2016(1):254
- Li D, Wu Y, Zhu M (2017) Nonbinary LDPC code for noncoherent underwater acoustic communication under non-Gaussian noise. In: Paper presented at the signal processing, communications and computing (ICSPCC), 2017 IEEE International Conference on
- Liu L, Wang Y, Li L, Zhang X, Wang J (2009) Design and implementation of channel coding for underwater acoustic system. In: Paper presented at the ASIC, 2009. ASICON'09. IEEE 8th international conference on
- Liu L, Zhang Y, Zhang P, Zhou L, Niu J (2017) Channel coding for underwater acoustic single-carrier CDMA communication system. In: Paper presented at the seventh international conference on electronics and information engineering
- Liu Y, Chen X, Zhong Z, Ai B, Miao D, Zhao Z et al (2017) Waveform design for 5g networks: analysis and comparison. *IEEE Access* 5:19282–19292
- Medwin H, Clay CS (1997) *Fundamentals of acoustical oceanography*. Academic Press, Cambridge
- Murugan SS, Natarajan V (2010) Performance analysis of signal to noise ratio and bit error rate for multiuser using passive time reversal technique in underwater communication. In: Paper presented at the 2010 international conference on wireless communication and sensor computing (ICWCSC)
- Noguet D, Gautier M, Berg V (2011) Advances in opportunistic radio technologies for TVWS. *EURASIP J Wirel Commun Netw* 2011(1):170
- Ochiai H, Imai H (2001) On the distribution of the peak-to-average power ratio in OFDM signals. *IEEE Trans Commun* 49(2):282–289
- Panaro J, Lopes F, Barreira LM, Souza FE (2012) Underwater acoustic noise model for shallow water communications. In: Paper presented at the Brazilian telecommunication symposium
- Qiao G, Babar Z, Ma L, Liu S, Wu J (2017) MIMO-OFDM underwater acoustic communication systems—a review. *Phys Commun* 23:56–64
- Roy S, Duman TM, McDonald V, Proakis JG (2007) High-rate communication for underwater acoustic channels using multiple transmitters and space-time coding: receiver structures and experimental results. *IEEE J Oceanic Eng* 32(3):663–688
- Schaich F, Wild T (2014) Waveform contenders for 5G—OFDM vs. FBMC vs. U-FMC. In: Paper presented at the 2014 6th international symposium on communications, control and signal processing (ISCCSP)
- Sha'ameri AZ, Al-Aboosi YY, Khamis NHH (2014) Underwater acoustic noise characteristics of shallow water in tropical seas. In: Paper presented at the computer and communication engineering (ICCCE), 2014 international conference on
- Shah NSM, Al-Aboosi YY, Ahmed MS (2018) Error performance analysis in underwater acoustic noise with non-Gaussian distribution. *Telkomnika* 16(2):681–689

- Stojanovic M, Preisig J (2009) Underwater acoustic communication channels: propagation models and statistical characterization. *IEEE Commun Mag* 47(1):84–89
- Stojanovic M, Catipovic JA, Proakis JG (1994) Phase-coherent digital communications for underwater acoustic channels. *IEEE J Oceanic Eng* 19(1):100–111
- Tahir B, Schwarz S, Rupp M (2017) BER comparison between convolutional, turbo, LDPC, and polar codes. In: Paper presented at the telecommunications (ICT), 2017 24th international conference on
- Urick RJ (1984) Ambient noise in the sea. Report No. 20070117128. Undersea Warfare Technology Office, Naval Sea Systems Command, Washington DC
- Wang J, Jin A, Shi D, Wang L, Shen H, Wu D et al (2017) Spectral efficiency improvement with 5G technologies: results from field tests. *IEEE J Sel Areas Commun* 35(8):1867–1875
- Wu X, Jiang M, Zhao C (2018) Decoding optimization for 5G LDPC codes by machine learning. *IEEE Access* 6:50179–50186
- Zhang X, Jia M, Chen L, Ma J, Qiu J (2015) Filtered-OFDM-enabler for flexible waveform in the 5th generation cellular networks. In: Paper presented at the global communications conference (GLOBECOM), 2015 IEEE

Publisher's Note Springer Nature remains neutral with regard to jurisdictional claims in published maps and institutional affiliations.